An Adaptive Speed Term Based on Homogeneity for Level-set Segmentation

Yinpeng Jin[a], Andrew Laine[*a] and Celina Imielinska[b]

[a] Department of Biomedical Engineering, Columbia University, New York, NY
[b] Office of Scholarly Resources, Department of Medical Informatics and Department of Computer Science, Columbia University, New York, NY

ABSTRACT

We studied an edge map computed from a local homogeneity measurement, as a replacement for the traditional gradient-based edge map applied in level-set segmentation methods. In existing level-set techniques, the gradient information is used as a stopping criteria for curve evolution, and also provides the attracting force to the zero level-set from a target boundary. However, in a discrete implementation, the gradient-based term can never fully stop the level-set evolution even for ideal edges, making leakage often unavoidable. Also the effective distance of the attracting force and blurring of edges become a design trade-off in choosing the shape and support of the smoothing filter. The proposed homogeneity measurement provides easier and more robust edge estimation, and makes possible the full stopping of level-set evolution. The homogeneity speed term decreases from a homogenous region to the boundary, which dramatically increases the effective distance of the attracting force and also provides an additional measurement of the overall approximation to the target boundary. Therefore, it provides a reliable criteria for adaptively changing the advent speed. By using this term, the leakage problem was avoided effectively in most cases compared to traditional level-set methods. The computation of the homogeneity is fast and its extension to the 3D case is straightforward.

Keywords: Level set, Image Segmentation, Homogeneity, Edge Map.

1. INTRODUCTION

1.1 Curvature evolution and Level set

Segmentation of medical images is an important step in applications such as visualization, quantitative analysis and image-guided surgery. Numerous segmentation methods have been developed. Traditional methods, such as pixel-based clustering, region growing, and edge detection require additional pre-processing and post-processing as well as a considerable amount of expert intervention and/or *a prior* information of an object of interest. Furthermore the subsequent analysis of segmented objects is often hampered by low-level pixel or voxel level representations of region-based segmentation [1].

Deformable models, on the other hand, provide an explicit representation of the boundary and the shape of an object. They combine several desirable features such as inherent connectivity and smoothness, which counteract noise and boundary irregularities, as well as the ability to incorporate knowledge about an object of interest [2, 3, 4]. However, parametric deformable models have two main limitations. First, in situations where an initial model and a desired object boundary differ greatly in size and shape, the model must be reparameterized dynamically to faithfully recover the object boundary. The second limitation is difficulty in dealing with topological adaptation such as splitting or merging model parts, a useful property for recovering either multiple objects or an object with unknown topology. This difficulty is caused by the fact that a new parameterization must be constructed whenever a topology change occurs, which requires sophisticated schemes [5, 6].

Level set segmentation [7, 8], or geometric deformable models, provides an elegant solution to address the primary limitations of parameteric deformable models. In the 2D case, the boundary of an object is implicitly represented as the zero-level set of a time dependent 2D function, which is usually called the level set function. A useful property of this

* Correspondence: Email: laine@columbia.edu

Medical Imaging 2002: Image Processing, Milan Sonka, J. Michael Fitzpatrick,
Editors, Proceedings of SPIE Vol. 4684 (2002) © 2002 SPIE · 1605-7422/02/$15.00

approach is that the level set function remains a valid function while the embedded curve (the zero level set) can change its topology.

The evolution equation for the level set function $\phi(x, y, t)$ takes the following formula [9]:

$$\frac{\partial \phi}{\partial t} + F\left|\nabla \phi\right| = 0. \qquad (1)$$

The evolution of the level set function is determined by the speed function *F*. As an example, imagine an initial closed curve that is evolving under three simultaneous motions. First, it is expanding with a constant speed in its normal direction; second, it is moving with a speed proportional to its curvature; third, it is being passively advected by an underlying velocity field whose direction and strength depend on position and time, but not on the front itself. This entire motion can then be written in terms of the speed function as an explicit level set scheme:

$$F = F_{prop} + F_{curv} + F_{adv}. \qquad (2)$$

where $F_{prop} = F_0$ is the propagation expansion speed, $F_{curv} = -\varepsilon\kappa$ is the dependence of the speed on the curvature κ, and $F_{adv} = \vec{U}(x, y, t)\bullet\vec{n}$ is the advection speed, where $\vec{n}$ is the normal to the front. The PDE in (1) can be solved with entropy-satisfying schemes given the speed function.

A small modification of (2) gives the general formula for level set segmentation:

$$\phi_t + g_I(1-\varepsilon\kappa)\left|\nabla \phi\right| - \beta\nabla P\bullet\nabla\phi = 0. \qquad (3)$$

In the term $1-\varepsilon\kappa$, the uniform expansion with speed 1 corresponds to the inflation force used by Cohen [10]. The diffusive term $\varepsilon\kappa$ smooths out the high curvature regions and has the same regularizing effect as the internal deformation energy term in thin-plate-membrane splines [2]. The term g_I was computed from the image data, and provides a halting criterion for the speed function. The value of g_I is between 0 and 1, and ideally, is 0 on the boundary and 1 within a homogeneous region (either within or outside an object). Typically, g_I is estimated by computing the gradient:

$$g_I(x, y) = \frac{1}{1+\left|\nabla(G_\sigma * I(x, y))\right|}. \qquad (4)$$

where the expression $G_\sigma * I$ denotes the image convolved with a Gaussian smoothing filter whose characteristic width is σ. The term $\nabla(G_\sigma * I(x, y))$ is essentially zero except where the image gradient changes rapidly, in which case the value becomes large. Thus, g_I is close to unity away from boundaries and drops to zero near sharp changes in the image gradient. These changes presumably correspond to the edges of a desired shape. In other words, the first term in (3) anticipates steep drops in the image gradient, and retards the evolving front from passing out of the desired region. The second term in (3) is a force which attracts the surface towards the boundary, which has a stabilizing effect, especially when there is a large variation in the image gradient value. This term denotes the projection of an attractive force vector on the surface normal. This force, introduced in [11], is realized as the gradient of a potential field. Here

$$P = -\left|\nabla(G_\sigma * I)\right|. \qquad (5)$$

attracts the surface to edges in the image, and the coefficient β controls the strength of this attraction.

Apparently, both terms depend on the edge map $\nabla(G_\sigma * I)$, and the quality of this edge estimation determines the performance of the segmentation.

1.2 "Scale Map" based on homogeneity measurement

"Scale" is a fundamental, well-established concept in image processing [12, 13]. The premise behind this concept is to consider the local size of an object in carrying out whatever local operations that are done on the image. We use this as a measure of local homogeneity [13].

"Object Scale" in an image *C* at any pixel *c* was defined as the radius *r(c)* of the largest hyperball centered at *c* which lies entirely in the object region [14].

A hyperball $B_r(c)$ centered at pixel *c* is a collection of pixels around *c*, i.e. $B_r(c) = \{e \in C \mid \|c - e\| \le r\}$. For a ball $B_k(c)$ of any radius *k* centered at *c*, a fraction function $FO_k(c)$ was defined, which indicates whether the fraction of the ball boundary is sufficiently homogeneous with respect to the inside region of the ball.

The fraction function applied was

$$FO_k(c) = \frac{\sum_{d \in B_k(c) - B_{k-1}(c)} W(|f(c) - f(d)|)}{|B_k(c) - B_{k-1}(c)|} \qquad (6)$$

where $|B_k(c) - B_{k-1}(c)|$ is the number of pixels in $B_k(c) - B_{k-1}(c)$ and *W* is the homogeneity function, which measures the similarity of two pixels based on their pixel value in an image *f(x)*. Examples of typically used homogeneity functions are illustrated in Figure 1.

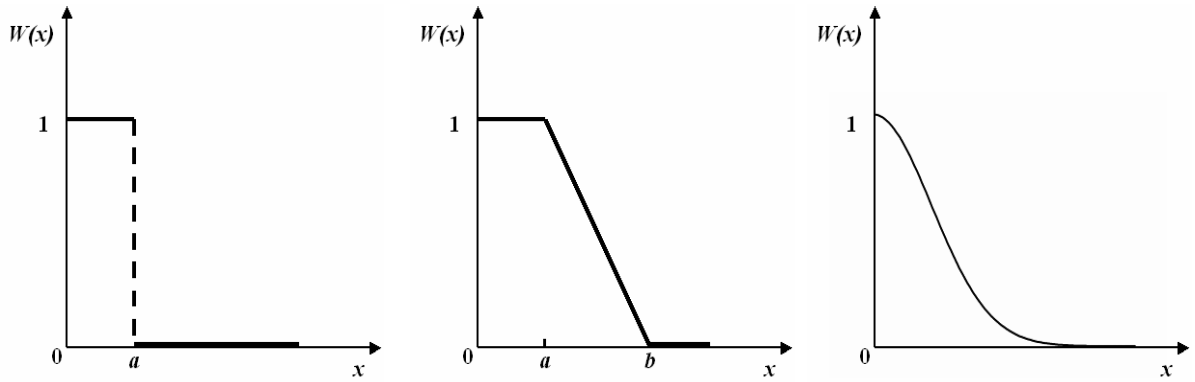

(a) (b) (c)

Figure 1: Typical homogeneity functions for computing the fraction function in Eqn. (6).

The mathematical formula for the homogeneity functions in Figure 1 are:

(a) $W(x) = \begin{cases} 1, & 0 \le x \le a \\ 0, & x > a \end{cases}$

(b) $W(x) = \begin{cases} 1, & 0 \le x \le a \\ \dfrac{b-x}{b-a}, & a \le x \le b \\ 0, & x > b \end{cases}$ (7)

(c) $W(x) = e^{-x^2/2k^2}, k > 0$

By setting a fixed threshold $0 < t < 1$, the scale map at a pixel *c* can be computed by the following pseudo-code:

```
begin
    k=1;
    while FO_k(c) ≥ t do
        k=k+1;
    endwhile
    r(c)=k;
end
```

2. METHOD

2.1 Edge Map based on homogeneity measures

The scale map in section 1.2 provides a robust homogeneity measurement by incorporating a tolerance level *t*. As an example, if we use $t = 7/8$, in a 3×3 neighborhood of a pixel *c* in a 2D scene, we allow one out of the eight neighboring pixels to belong to a different object (to account for noise) and would still consider the neighborhood to be entirely within the same object. This actually provides a mechanism of denoising within the homogeneity measurement.

An edge was defined as a region of an image in which the pixel value changes significantly over a short distance [15]. Therefore the edge represents the region that has significant lower homogeneity. In this case, the homogeneity measurement provides the edge information in an image.

Figure 2 shows the "scale map" computed by the algorithm in section 1.2 using selected parameters.

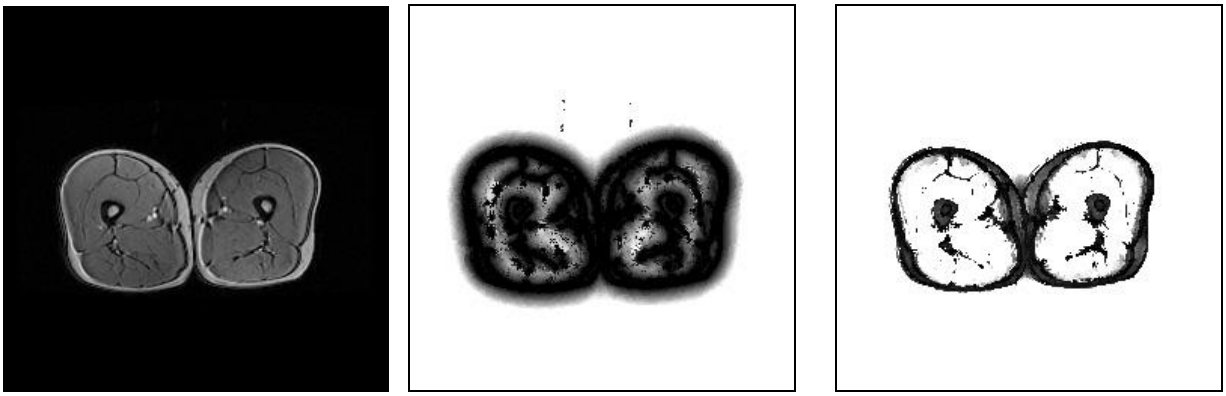

(a) (b) (c)

Figure 2: Scale map of an MRI image of thighs. (a) Gray scale image (with 256 gray levels). (b),(c) Scale map with distinct parameters. (b): k^2 =500, t=0.8. (c): k^2 =1200, t=0.5.

Here we use Eqn. 7(c) as the homogeneity function. The parameters for computing the scale map are the shape parameter of the homogeneity function (*k*), and the tolerance value for homogeneity measurement (*t*). The parameter *k* determines how much of the variations in a pixel value will be tolerated in terms of homogeneity. *t*. As discussed previously, *t* determines how much noise we want to ignore. Figure 2(b) used a smaller *k* and larger *t* values comparing to Figure 2(c).

Figure 2(b) and (c) show the appearance of an edge map with lower values on the boundary and higher values on the homogeneous region. As stated in Section 1.1, if we scaled the pixel value of this edge map to [0,1], it may be used as an image-based term for level set segmentation.

2.2 Level set segmentation using the homogeneity edge map

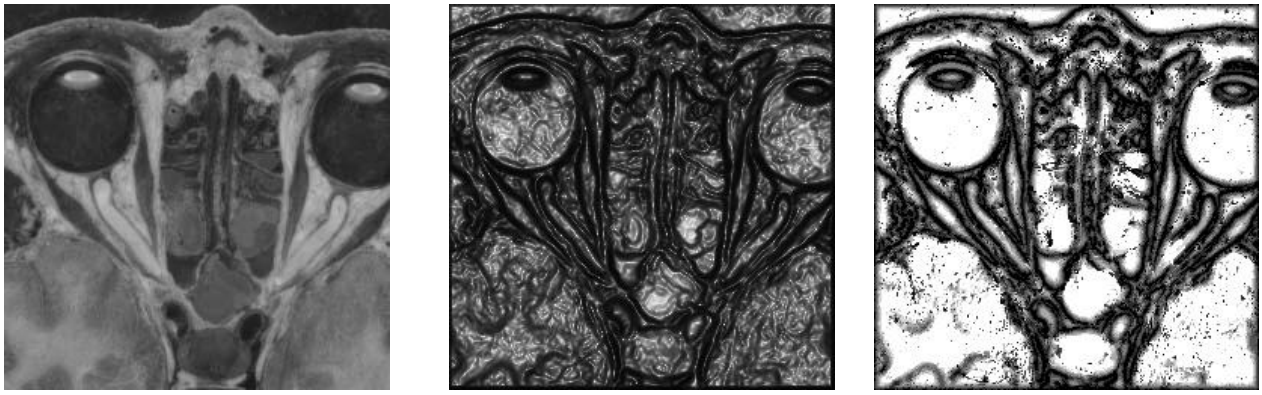

(a) (b) (c)

Figure 3: (a) Gray scale image from Visible Human Dataset. (b) Edge map computed from the gradient of gaussian filter as in (4). (c) Edge map computed from the homogeneity measurement.

Figure 3 shows a comparison of edge maps computed from the gradient and the proposed homogeneity measures. Notice that even in the relatively homogenous region, e.g. within the eyeball, the gradient edge map has a lot of noise, but in the homogeneity edge map, because of the build-in tolerance on noise level, removes small amounts of noise, and therefore provides a "clean" map in homogeneous regions.

Revisiting the level set evolution function (3), without the attracting speed term, we have:

$$\phi_t + g_I |\nabla \phi| - g_I \varepsilon \kappa |\nabla \phi| = 0. \qquad (8)$$

The first term in (8) provides an expansion speed along the normal direction of the curve. Therefore, in the non-boundary region, we want the edge map magnitude g_I to be as large as possible, so that the curve evolution can be converge to the real boundary quickly. Looking at Figure 3(b), the edge map has significant noise inside the object region, therefore dramatically slows down evolution of the curve. This can be seen in the comparison of Figure 4 and Figure 5.

Ideally, g_I will be zero on the estimated boundary, so that when the curve reaches it, the evolution function becomes $\phi_t = 0$, and attains equilibrium. But since the gradient $\nabla(G_\sigma * I)$ will never be infinite in a discrete implementation, g_I will never be exactly zero. This is why extra efforts are always needed to stop the level set evolution when it reaches an estimated boundary.

In this research, we used an edge map defined by measuring homogeneity. The value of the edge map can be zero on a sharp boundary. It provided a more reliable stopping criteria. But because of the existence of the noise tolerance, a weak boundary still could be non-zero. Also, missing boundaries as frequently occurs in medical images, these will result in boundary leakage if the boundary definition in the original image is not perfectly clear. An attracting term (5) introduced in [11] is used to pull back the curve when it passes the boundary. We added an adaptive indication term that shuts down the expansion speed when the curve becomes close enough to the estimated boundary. The evolution function we used is:

$$\phi_t + g_I \cdot \delta \cdot |\nabla \phi| - \varepsilon \kappa |\nabla \phi| - \beta \nabla P \cdot \nabla \phi = 0. \qquad (8)$$

The reason we take out g_I from the second term is that as the curve approaching the boundary, the value of g_I became very small, therefore the smoothing effect was eliminated. When using the attracting term, the curve always appears noisy due to imperfect boundaries in the edge map. This is a direct analogy of parametric deformable models that always keep a constant weighted elastic internal force.

δ is an global indication function such that when the zero level set of ϕ is close enough to the estimated boundary, $\delta = 0$ and otherwise $\delta = 1$. Considering the computation of the homogeneity map, it is intuitive to see that pixel values in the edge map decreases from the homogeneous region to the boundary, and reaches a minimum at the boundary. Therefore the pixel value of the edge map actually gives the information of how close a certain pixel is to the boundary. By averaging the values in the edge map over the pixels that represent the zero level set, or finding the maximum value, we can find how close the whole curve is closing to the target boundary. A threshold is chosen so that when this value is smaller than the threshold $\delta = 0$, and otherwise $\delta = 1$.

Figure 4 shows a boundary leakage problem when using the gradient edge map along with the presence of an attracting term. By using the proposed speed term, the evolution is faster and the leakage problem was solved.

3. DISCUSSION

The major problem of level set segmentation is boundary leakage when a weak boundary or missing part of a boundary occurs. Efforts have been made to add extra stopping criteria [16] or region information [17, 18]. When dealing with weak boundaries, sometimes the expansion term was removed [19], while an initialization that is close to the boundary was needed. In this research, we kept the expansion term initially for pushing the model approaching the boundary, therefore no restriction on initialization was needed. When the expansion term was shut down, it prevented boundary leakages.

The definition of this homogeneity measurement does not include any requirement on dimensions, and therefore can be easily extended to higher dimension. It is also computationally efficient because no filtering/convolution is involved. In addition, collecting all the pixels around the zero level set for computing the indication function δ is a by-product when constructing the extension speed when iterating the level set function. Therefore this test can be done whenever the construction of extension speed is performed without much extra computation.

Since this research proposed a new edge map, other research efforts on speed terms based on edge maps [16, 20] can be investigated straightforward to achieve more reliable level set evolution and segmentation. Future work should be focused on extensions to higher dimension and building other desirable speed term based on edge maps or other information derived from of the underlining image.

ACKNOWLEDGMENTS

This research was supported in part by the NLM contract of Image Segmentation and Registration Toolkit (ITK), and The Whitaker Foundation.

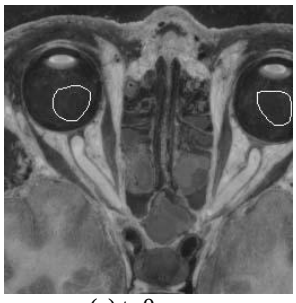
(a) t=0

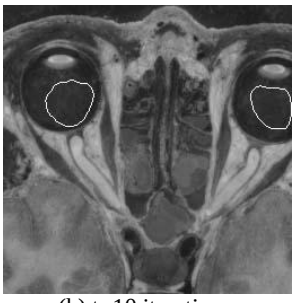
(b) t=10 iterations

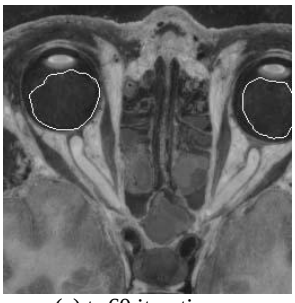
(c) t=60 iterations


(d) t=110 iterations

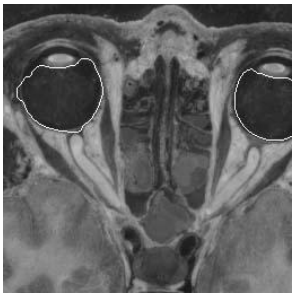
(e) t=130 iterations


(f) t=190 iterations

Figure 4: level-set evolutions using image-base speed in Figure 3(b).

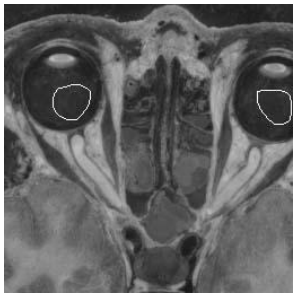
(a) t=0

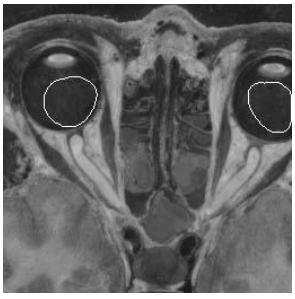
(b) t=10 iterations

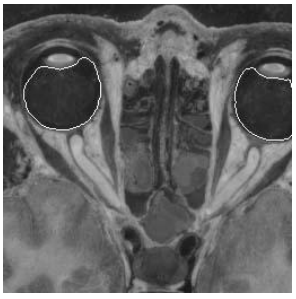
(c) t=60 iterations

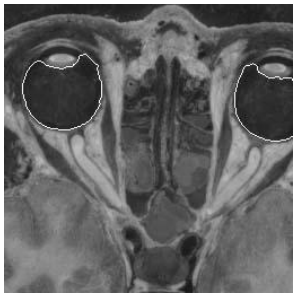
(d) t=80 iterations


(e) t=130 iterations


(f) t=190 iterations

Figure 5: level-set evolutions using image-base speed in Figure 3(c).

REFERENCE

[1] T. McInerney and D. Terzopoulos, "Deformable models in medical image analysis: A survey," *Medical Image Analysis*, vol. 1, pp. 91-108, 1996.

[2] M. Kass, A. Witkin, and D. Terzopoulos, "Snakes: Active contour models," *International Journal of Computer Vision*, vol. 1, pp. 321-331, 1987.

[3] D. N. Metaxas, *Physics-based deformable models. Applications to computer vision, graphics and medical imaging*, 1997.

[4] C. Xu, D. Pham, and J. Prince, "Image segmentation using deformable models.," in *Handbook of Medical Imaging*, vol. 2: SPIE, 2000, pp. 129-174.

[5] T. McInerney and D. Terzopoulos, "Topologically adaptable snakes," presented at 5th International Conference on Computer Vision, 1995.

[6] R. Durikovic, K. Kaneda, and H. Yamashita, "Dynamic contour: a texture approach and contour operations," *The Visual Computer*, vol. 11, pp. 277-289, 1995.

[7] S. Osher and J. A. Sethian, "Fronts propagating with curvature-dependent speed: Algorithms based on Hamilton-Jacobi formulations," *Journal of Computational Physics*, vol. 79, pp. 12-49, 1988.

[8] R. Malladi, J. A. Sethian, and B. C. Vemuri, "Shape modeling with front propagation: A level set approach," *IEEE Transactions on Pattern Analysis and Machine Intelligence*, vol. 17, pp. 158-175, 1995.

[9] J. Sethian, *Level set methods and fast marching methods*, 1999.

[10] L. D. Cohen, "On active contour models and balloons," presented at Computer Vision, Graphics, and Image Processing: Image Understanding, 1991.

[11] V. Caselles, R. Kimmel, and G. Sapiro, "Geodesic active contours," presented at ICCV'95, 1995.

[12] M. Tabb and N. Ahuja, "Multiscal Image segmentation by integrated edge and region detection," *IEEE Transactions on Image Processing*, vol. 6, pp. 642-655, 1997.

[13] P. Saha and J. Udupa, "Scale-based fuzzy connectivity: a novel image segmentation methodology and its validation," presented at SPIE conference on Medical Imaging, 1999.

[14] P. Saha, J. Udupa, and D. Odhner, "Scale-based fuzzy connected image segmenation: theory, algorithms, and validation," *Computer Vision and Image Understanding*, vol. 77, pp. 145-174, 2000.

[15] K. R. Castleman, *Digital Image Processing*. Upper Saddle River, NJ: Prentice-Hall Inc., 1996.

[16] K. Siddiqi, Y. B. Lauziere, A. Tannenbaum, and S. W. Zucker, "Area and Length Minimizing Flows for Shape Segmentation," *IEEE Transactions on Image Processing*, vol. 7, pp. 433-443, 1998.

[17] A. Yezzi, A. Tsai, and A. Willsky, "A statistical approach to image segmentation for biomodal and trimodal imagery.," presented at ICCV, 1999.

[18] N. Paragios and R. Deriche, "Geodesic active contours and level sets for the detection and tracking of moving objects," *IEEE Transactions on Pattern Recognition and Machine Intelligence.*, vol. 22, pp. 1-15, 2000.

[19] A. Sarti and R. Malladi, "A Geometric Level Set Model for Ultrasounds Analysis," University of California, Berkeley LBNL-44442, 1999.

[20] C. Xu and J. L. Prince, "Snakes, Shapes and Gradient Vector Flow," *IEEE Transaction on Image Processing*, pp. 359-369, 1998.